Journal of Cerebral Blood Flow & Metabolism (2010) 30, 440–448

www.jcbfm.com

Sepsis-associated encephalopathy: a magnetic resonance imaging and spectroscopy study

Fernando A Bozza[1,2], Philippe Garteiser[3], Marcus F Oliveira[2,4], Sabrina Doblas[3], Rebecca Cranford[3], Debra Saunders[3], Inna Jones[3], Rheal A Towner[3] and Hugo C Castro-Faria-Neto[5]

[1]*ICU, Instituto de Pesquisa Clínica Evandro Chagas, Fundação Oswaldo Cruz, Rio de Janeiro, Brazil;* [2]*Laboratório de Inflamação e Metabolismo, Instituto Nacional de Ciência e Tecnologia de Biologia Estrutural e Bioimagem, Universidade Federal do Rio de Janeiro, Rio de Janeiro, Brazil;* [3]*Advanced Magnetic Resonance Center, Oklahoma Medical Research Foundation, Oklahoma City, Oklahoma, USA;* [4]*Programa de Biologia Molecular e Biotecnologia, Laboratório de Bioquímica Redox, Instituto de Bioquímica Médica, Universidade Federal do Rio de Janeiro, Rio de Janeiro, Brazil;* [5]*Laboratório de Imunofarmacologia, Instituto Oswaldo Cruz, Fiocruz, Rio de Janeiro, Brazil*

Brain dysfunction is frequently observed in sepsis as a consequence of changes in cerebral structure and metabolism, resulting in worse outcome and reduced life-quality of surviving patients. However, the mechanisms of sepsis-associated encephalopathy development and a better characterization of this syndrome *in vivo* are lacking. Here, we used magnetic resonance imaging (MRI) techniques to assess brain morphology and metabolism in a murine sepsis model (cecal ligation and puncture, CLP). Sham-operated and CLP mice were subjected to a complete MRI session at baseline, 6 and 24 h after surgery. Accumulation of vasogenic edematic fluid at the base of the brain was observed in T_2-weighted image at 6 and 24 h after CLP. Also, the water apparent diffusion coefficients in both hippocampus and cortex were decreased, suggesting a cytotoxic edema in brains of nonsurvival septic animals. Moreover, the *N*-acetylaspartate/choline ratio was reduced in brains of septic mice, indicating neuronal damage. In conclusion, noninvasive assessment by MRI allowed the identification of new aspects of brain damage in sepsis, including cytotoxic and vasogenic edema as well as neuronal damage. These findings highlight the potential applications of MRI techniques for the diagnostic and therapeutic studies in sepsis.
Journal of Cerebral Blood Flow & Metabolism (2010) **30,** 440–448; doi:10.1038/jcbfm.2009.215; published online 21 October 2009

Keywords: inflammation; infection; central nervous system; blood–brain barrier; delirium

Introduction

Although it is well accepted that the brain may be affected during sepsis, it was only recently shown that the presence of brain dysfunction impacts directly as an independent determinant of poor prognosis in patients with sepsis (Sprung *et al*, 1990; Ely *et al*, 2004; Lin *et al*, 2008). Growing evidence supports that an early central autonomic dysfunction contributes to the hemodynamic changes found in septic shock patients (Sharshar *et al*, 2003) and long-term cognitive impairment can be present in sepsis survivors (Siami *et al*, 2008). Sepsis-associated encephalopathy, or sepsis-associated delirium, is a diffuse cerebral dysfunction characterized by an acute onset of an impairment of cognitive function, which can vary from inattention, disorientation, agitation, stupor and coma. The animal model of sepsis using cecal ligation and puncture (the CLP model) is able to mimic clinical sepsis-associated encephalopathy as it induces autonomic dysfunction (Kadoi and Goto, 2004; Pancoto *et al*, 2008) and long-term cognitive impairment (Barichello *et al*, 2005).

Magnetic resonance imaging (MRI) techniques offer unique capabilities in observing morphologic and metabolic characteristics of the brain *in vivo*, and have been often applied in the characterization of acute or subacute encephalopathies (Penet *et al*,

Correspondence: Dr FA Bozza, Instituto de Pesquisa Clínica Evandro Chagas, Fundação Oswaldo Cruz, Av Brasil, 4365, Manguinhos, Rio de Janeiro, RJ 21040-900, Brazil.
E-mails: bozza.fernando@gmail.com or fernando.bozza@ipec.fiocruz.br
Supported in part by grants from Conselho Nacional de Desenvolvimento Científico e Tecnológico (CNPq, Brazil) and Fundação Carlos Chagas Filho de Amparo *à* Pesquisa do Estado do Rio de Janeiro (FAPERJ, Brazil), and Fundação Oswaldo Cruz.
Received 1 May 2009; revised 8 August 2009; accepted 14 September 2009; published online 21 October 2009

2005; Rosengarten *et al*, 2008; Testylier *et al*, 2007). In particular, diffusion-weighted imaging and apparent diffusion coefficient (ADC) mapping techniques are generally accepted modalities to noninvasively measure tissue and cellular damage, because of their high sensitivity. The relevance of measuring ADC lies on its potential to characterize water movement on cellular scales, such as the increased water content of the interstitial space associated with vasogenic edema, or the restricted intracellular water movement occurring in cytotoxic edema. In particular, techniques based on diffusion-weighted imaging have been used to examine cerebral edema for a variety of pathologies including focal cerebral ischemia (Kokubo *et al*, 2002; Walker *et al*, 2004) and brain tumors (Eis *et al*, 1995; Server *et al*, 2009) both in human studies and in animal models.

In addition, MRI offers the unmatched possibility of acquiring quantitative data on a subset of metabolites *in vivo* over time during a pathogenic process. The monitoring of relative levels of total choline (Ch), total creatine (Cr), and *N*-acetylaspartate (NAA) would be especially relevant to sepsis. Choline is an important component of cellular membrane phospholipids, where measurements of total Ch levels represent a sensitive, though indirect, marker of the cellular death (Blankenberg *et al*, 1997; Sibtain *et al*, 2007). Creatine levels are also valuable because they are related to cerebral energy metabolism (Sibtain *et al*, 2007), which would be expected to be perturbed because of the mitochondrial dysfunction in sepsis (d'Avila *et al*, 2008). Finally, NAA is recognized as a marker of neuronal damage (Ross and Bluml, 2001) and decreases of its levels have been associated with neuronal loss (Birken and Oldendorf, 1989; Moffett *et al*, 2007; Vuori *et al*, 2004) in various pathologies including sepsis (Orihuela *et al*, 2006).

Here, we used MRI and spectroscopy techniques to monitor the consequences of a septic challenge to the mouse brain. Measurements in septic mice brains consisted of T_2-weighted imaging, to assess brain morphology, ADC mapping, to determine the respective contributions of cytotoxic or vasogenic processes, and proton spectroscopy, to gather information on the relative amounts of Ch and Cr containing metabolites and NAA. The data presented here support the notion that early sepsis is associated to encephalopathies involving neuronal damage and cytotoxic edema.

Materials and methods

Experimental Design

Mice were first subjected to an MRI session during which baseline values were acquired. Animals were then subjected to CLP surgery or sham operation. A complete MRI data set was acquired during the development of sepsis at 6 h after surgery. After the MRI session, animals were kept for at least 18 h. For animals that were still alive 24 h after surgery, we acquired a second MRI data set at that time point.

Cecal Ligation and Puncture Model

The CLP protocol was approved by the Institutional Animal Care and Use Committee and performed in accordance to the guidelines set out by the National Institutes of Health. Cecal ligation and puncture was performed as previously described (Gomes *et al*, 2006). Sixteen 8- to 10-week-old male C57BL/6 mice were anesthetized with isoflurane (2% to 3%) under aseptic conditions. A laparotomy was performed with a 2 cm midline incision through the linea alba. The cecum was exposed and ligated with sterile 3-0 silk below the ileocecal junction. The cecum was punctured once with an 18-gauge needle and squeezed to empty its content through the puncture. The cecum was returned to the peritoneal cavity, and the abdominal muscle and skin incisions were closed. After the surgery, 0.5 mL of sterile saline was administered subcutaneously to the animals. Mice in the sham operation group were subjected to identical procedures, except that ligation and puncture of the cecum were omitted. The lethality of our model was approximately 40% in the first 24 h and 60% in 144 h.

Magnetic Resonance Imaging

Mice were anesthetized using 2% isoflurane and 800 mL/min oxygen, and maintained with a constant body temperature of 37°C under general anesthesia using 1% isoflurane during the imaging session. Their respiratory rate was monitored. All MRIs were acquired on a 7 T, 30 cm horizontal bore magnet (Bruker Biospin, Ettlingen, Germany), using a G060 gradient set and a whole-body multi-rung 38 mm resonator.

Morphologic Images

Morphologic images were acquired using a rapid acquisition, relaxation-enhanced pulse sequence with T_2 weighting (repetition time, 4 secs; echo time, 56 ms; flip angle, 90°) and a rapid acquisition, relaxation-enhanced factor of 8. The slice geometry was 15 contiguous axial slices of 25×25 mm and 1 mm in thickness, encoded into 192×192 matrices, resulting in a 130 μm in-plane resolution. Six averages were acquired, yielding total acquisition times of 8 mins. In animals where accumulation of edematic fluid was observed at the base of the brain, regions of interest were manually outlined using the native regions of interest tool of the magnet operating software (ParaVision; Bruker Biospin, Ettlingen, Germany). These regions were traced for each slice between the rostral end of the olfactive bulb and the hippocampus. The corresponding areas were summed together and multiplied by the slice thickness to yield a volume in cubic millimeters. To suppress operator bias, the manual outlining step of edematic areas was repeated by three independent operators with no knowledge of the condition of each animal. No statistical differences were found between the values obtained by the different observers.

Diffusion-Weighted Imaging

Diffusion-weighted images were acquired using a single-shot echo-planar encoded imaging sequence with a repetition time of 1,325 ms, an echo time of 63 ms, and a flip angle of 90°. Geometric distortions inherent to this encoding scheme applied at an operating proton frequency of 300 MHz were greatly diminished by careful shimming of the volume of interest using the 'fast automatic shimming technique by mapping along projections' method (Gruetter, 1993). The diffusion-sensitizing scheme of Stejskal and Tanner (1965) was used. Diffusion-sensitizing gradients (7 ms) were applied along the rostro-caudal axis, separated by 14 ms and located at symmetric positions on either side of the refocusing pulse. Five images were obtained with different gradient gains, resulting in b values of 0, 400, 800, 1,200, and 1,600 secs/mm^2. Seven contiguous square slices ($25.6 \times 25.6 \times 1\,mm^3$) were acquired and encoded in a 128×128 matrix, resulting in a 200 μm in-plane resolution. For each voxel, the signal intensities measured at different b values, $S(b)$, were numerically fitted against the model, $S(b) = S(b=0)\ e^{(-b.ADCx)}$. Similar results were obtained when linear regression was performed on the linearized version of this equation. All calculations were performed using a Mathematica (Wolfram Scientific, Champaign, IL, USA) program developed in-house. The resulting values for the axial component of the apparent diffusion coefficient tensor (ADC_x) were then used to generate colored parametric maps using a linear color scale ranging from 1×10^{-4} mm^2/sec (blue) to 1×10^{-3} mm^2/sec (red). For display purposes, voxels whose values were below or above this range were colored blue or red, but in subsequent calculations their values were not thresholded in any way. Regions of interest were traced for the cortex and thalamus, using the diffusion-weighted image with the lowest b value and a mouse anatomical atlas (Franklin and Paxinos, 1997). The ADC values of each voxel in these regions were averaged, and resulted in average ADC values for cortex and thalamus. Statistical analyses were subsequently carried out on these averages.

In Vivo Proton Spectroscopy

Proton spectra were acquired over a $3 \times 3 \times 3\,mm^3$ cube region located on the hippocampus. The point-resolved spectroscopy pulse sequence (90°-90°-180°) was used in combination with the variable power with optimized relaxation delays scheme of water suppression. A total of 256 averages were acquired with a repetition time of 2.5 secs and an echo time of 2×10 ms over a spectral width of 4,006 Hz (13.3 p.p.m.). The resulting decays were applied a line broadening noise reduction and were Fourier–transformed. The spectra were phased and zero-order baseline was corrected. Because the water peak had been suppressed, the spectra were calibrated with the easily recognizable peak of Ch (3.2 p.p.m.). After ascertaining that the overall aspect of the spectra was similar, analysis was carried out on a 3.5 p.p.m. spectral window where changes were identified, which contained the peaks for Ch compounds (3.21 p.p.m.), Cr compounds (3.03 p.p.m.) and NAA (2.02 p.p.m.) (Pfeuffer *et al*, 1999). These were fitted against a Gaussian lineshape, which was integrated to yield the peak area. In an effort to limit the sensitivity to phasing artifacts, we computed metabolite ratios for analysis. Although approximately 10 metabolite peaks were routinely identified, only the Cr, Ch, and NAA peaks were analyzed because of their superior peak area-to-noise ratio and clinical relevance.

Statistical Analyses

The statistical analysis was performed using the paired two-tailed Student's t-test to compare data from the same animal at baseline versus 6 h and an unpaired two-tailed Student's t-test for comparison between survivors and nonsurvivors. Normal distribution of data was tested with Kolmogorov–Smirnov test. Values are reported as means ± s.e.m. The program GraphPad Prism (version 4.00 for Windows; GraphPad Software, San Diego, CA, USA) was used to calculate P-values. Differences between groups were considered statistically significant when the associated P-values were less than 0.05.

Results

The brains of the septic mice were observed before surgical procedures, 6 h, and 24 h after surgery through MRI of axial slices with T_2 weighting. Figure 1 shows that septic animals developed a distinctive feature of a hyperintense area visible in the vicinity of the large vessels present at the base of the brain. The volumes associated with this local hyperintensity were measured at all available time points and we observed an increase of volume to approximately 4.6 mm^3 at 6 h after surgery in septic animals (Figure 2A). A significant difference was also found in the volume of the basal brain hyperintensity at 6 h between animals survived (3.4 mm^3) and not survived until the end point of our experiments (8.6 mm^3), with a P-value of 0.023 (Figure 2B).

The ADCs in the brain tissue of septic animals were compared with sham animals. Regions of interest were traced on the cortex and the thalamus using the diffusion-weighted images, and were reported on the ADC maps (Figure 3). The ADCs were averaged over these regions of interest, resulting in the observed values. In general, septic animals were found to have a diffuse decrease in the ADC. When separating CLP-operated animals according to their 24 h survival outcome, an important difference was found in the magnitude of the ADC decrease observed in both cortex and thalamus. Thus, sepsis-related deaths were linked with a decrease in the ADC values in the cortical and thalamic areas. On the ADC maps, the regions of T_2 hyperintensity found at the base of the brain during morphologic imaging were also distinctive, because they were hyperdiffusive (arrows, Figure 4). This indicates that the region

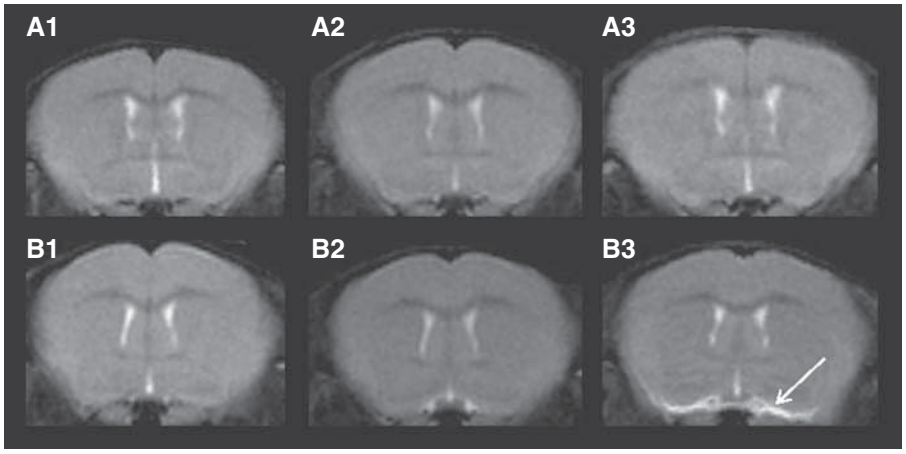

Figure 1 T_2-weighted axial MRI of representative brains from a sham-operated (**A**) and a CLP-operated (**B**) mice. The images were submitted to a Gaussian filtering of six pixels in radius. 1, baseline; 2, 6 h after surgery; and 3, 24 h after surgery. Accumulation of edematic fluid is visible as hyperintense area emanating from the blood vessels at the base of the brain in B2 and more evident in B3 (arrow).

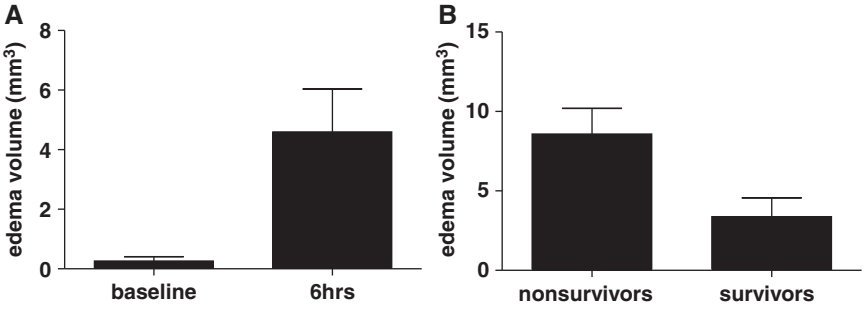

Figure 2 Basal brain-vessel-associated edema volumes (in mm^3) as measured on T_2-weighted images. (**A**) Volume measured before the CLP (baseline, $n = 15$, $0.27 \pm 0.14\,mm^3$) versus volume measured 6 h after CLP (6 h, $n = 14$, $4.6 \pm 1.44\,mm^3$). $^{**}P < 0.01$; paired Student's *t*-test. (**B**) volume measured at 6 h, sorted by animal survival. Nonsurvivors ($n = 5$, $8.6 \pm 1.61\,mm^3$) and survivors ($n = 11$, $3.4 \pm 1.195\,mm^3$). Data are presented as bars with mean ± s.e.m. values for each condition. $^{*}P < 0.05$ unpaired Student's *t*-test.

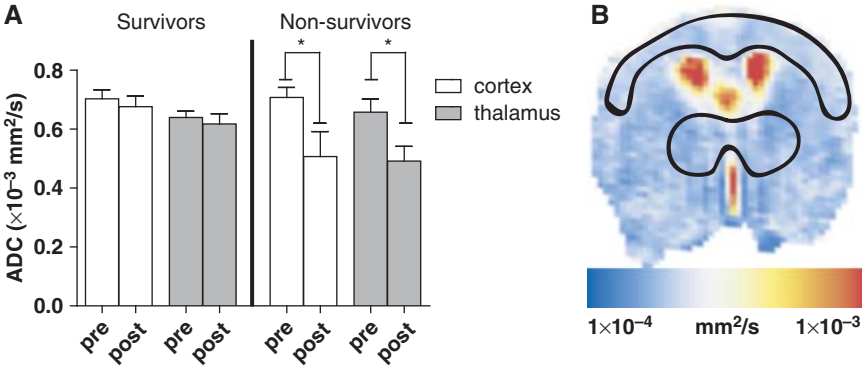

Figure 3 Apparent diffusion coefficients (ADCs). (**A**) Average ADC measured in the cortex and thalamus of survivor ($n = 11$) and nonsurvivor ($n = 5$) mice before (baseline) or 6 h after CLP (6 h). Data are presented as bars with mean ± s.e.m. values for each condition. $^{*}P < 0.05$; paired Student's *t*-test. (**B**) Representative ADC map as calculated from diffusion-weighted axial images. The black lines delineate the regions of interest represented for cortex and thalamus and were used to generate the average values reported in **A**.

peripheral to the Willis circle vessels underwent strong vasogenic edema event in lethal sepsis in mice.

Proton spectra (Figure 5A) were acquired in a cubic volume of 27 μL including the hippocampus, and the relative amounts of the total Cr, total Ch, and

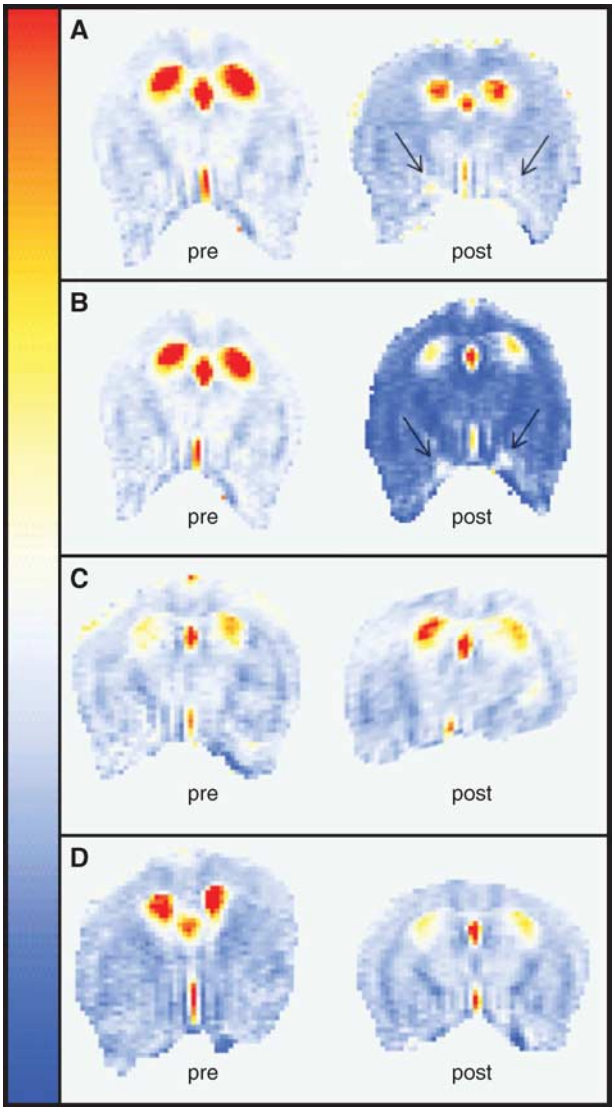

Figure 4 Representative apparent diffusion coefficient (ADC) maps before (baseline, left) and 6 h after (6 h, right) surgery. (**A** and **B**) Animals were septic and did not survive the challenge. They are shown to display the variance associated with ADC measures. (**C**) Example of an animal having undergone CLP but having survived the challenge. (**D**) Sham-operated animal. Black arrows: areas of hyperintense diffusion at the base of the brain. The color scale is represented on the left: blue, 1×10^{-4} mm^2/sec; red, 2×10^{-3} mm^2/sec.

NAA compounds were determined after the identification of their respective peaks (Figure 5B). A small increase was detected in the Cr/Ch ratio of septic animals (1.28 ± 0.14) 6 h after surgery compared with sham animals (1.04 ± 0.06). This change was not of sufficient amplitude to reach statistical significance given our sample size. A strong decrease was however seen in the NAA/Ch ratio, from a baseline value of 1.97 ± 0.15 to 1.39 ± 0.18 at 6 h after CLP. Overall, the results of our study could be explained by a decrease in NAA, although an increase in Ch levels concomitant with a greater increase in Cr levels could also result in the ratios that we observed. However, based on the individual aspect of the peaks, a decrease in NAA accompanied by relatively little changes in either Cr or Ch seems more likely.

Discussion

Although systematic MRI brain studies of sepsis are not yet available, recent preliminary investigations carried out in a small number of patients (Sharshar *et al*, 2007) and on animal models of endotoxemia (Rosengarten *et al*, 2008) highlighted the potential applications of MR techniques to determine the mechanisms of sepsis-associated encephalopathy. The noninvasiveness of MR techniques represents an important advantage to study temporal evolution of disease processes. In addition, these techniques also offer the ability to acquire *in vivo* data on morphology and physiology with negligible influence on the observed disease process. Recent improvements in computation power, field strengths, and hardware design have accelerated the appearance of robust and sensitive methods, which allow the detection of even small deviations from normal brain function in humans and animal models. Animal studies offer the unparalleled advantage of a more fully controlled experimental setting compared with human case studies, and are devoid of confounding influences such as demographic characteristics, risk factors, and prior treatment courses. Here we report the implementation of T_2-weighted imaging, ADC mapping, and proton spectroscopy in the mouse brain to put in evidence early changes induced by sepsis. Overall, we show that brain can be affected by distinct mechanisms resulting in cytotoxic and vasogenic edema as well as in neuronal damage. The results of our study contribute to the idea that the acquisition of such data *in vivo* in a clinically relevant model of sepsis provides valuable and novel information.

The data presented here also indicate that the brain damage in sepsis is characterized by disruption in the normal function of the blood–brain barrier and in cellular function as well. This was clearly apparent in the vicinity of blood vessels at the base of the brain as early as 6 h after disease onset, when edematic fluid accumulated therein. Also, fluid accumulation in the brain was strongly associated to the outcome at 24 h, although we could not establish a direct cause–effect relationship. We propose that this phenotype is a reliable marker of sepsis severity. The increase in vascular permeability observed here seems to be related to the systemic inflammation and the intensity of septic insult. Although animals were placed in a prone position, fluid accumulation was attributed to a leakage out of the vessels because it was systematically present in their vicinity, even when their volume was still small. However, we cannot discard a drainage effect from brain interstitial fluid to the base by gravity.

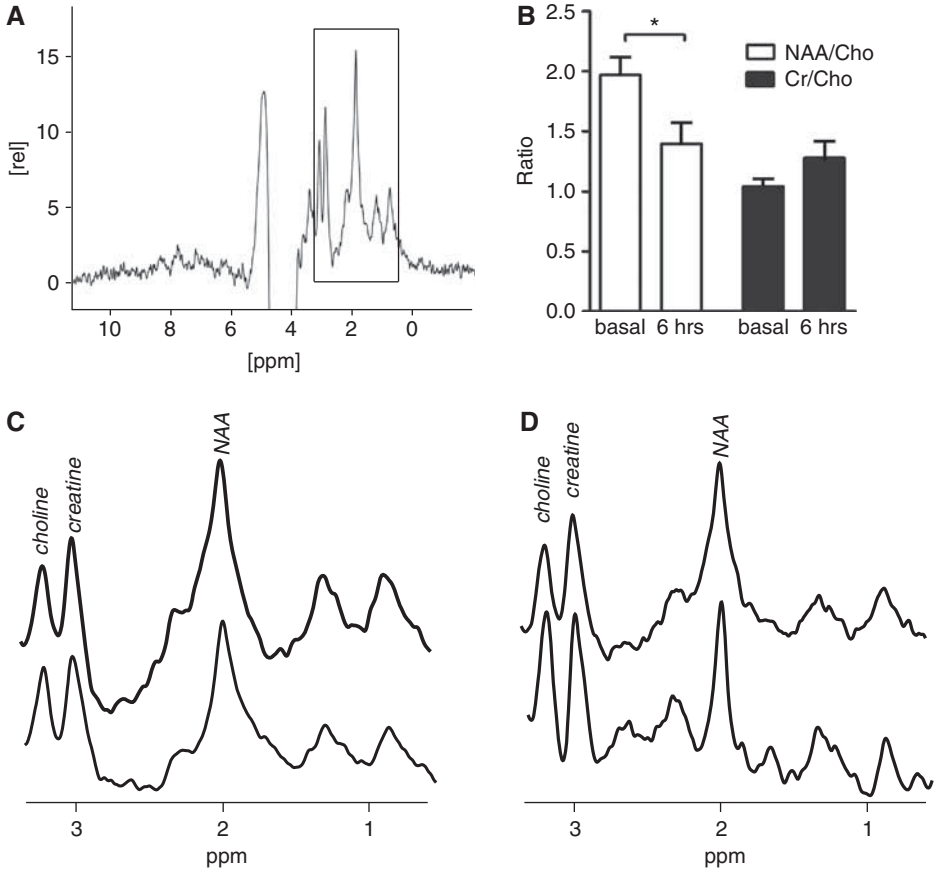

Figure 5 *In vivo* proton spectroscopic analysis of brain metabolites. (**A**) Representative spectra obtained at baseline. The spectral region used for quantification is outlined (black rectangle). (**B**) Average values ± s.e.m. of the peak area ratios of NAA to total choline (NAA/Cho, white bars) and total creatine to total choline (Cr/Cho, black bars) in our cohort of septic animals at baseline (basal) or 6 h after surgery (6 h). We observed a significant reduction in NAA/total choline ratio, with a paired Student's *t*-test *P*-value of 0.021 ($n = 11$). (**C** and **D**) Close-up views of the spectral region encompassing the choline, creatine, and NAA peaks for sham-operated (**C**) or CLP-operated (**D**) animals. Top trace, baseline spectrum; bottom trace, spectrum obtained 6 h after CLP. The peaks used in the calculation of the ratios are markedly visible at 3.21, 3.03, and 2.02 p.p.m. for total choline, total creatine, and *N*-acetylaspartate, respectively.

In the most prominent cases, fluid was visible on axial slices ranging from the most caudal section of the brain to the ventral side of the olfactory bulb. The development of cerebral edema often involves a sharp decrease in blood–brain barrier function (Papadopoulos *et al*, 2000). Compromised barrier integrity was evidenced in animal model and human sepsis by monitoring the levels or transport of various markers in the brain parenchyma (Jeppsson *et al*, 1981; Siami *et al*, 2008). Various cytokines released by activated leukocytes were shown to induce increased pinocytosis by endothelial cells (Anda *et al*, 1997; Huynh and Dorovini-Zis, 1993) and recently a central role of complement components (C5a) in blood–brain barrier dysfunction in sepsis was shown (Flierl *et al*, 2009).

Apparent diffusion coefficients measured in the cortex and thalamus of septic animals indicated alterations in this parameter, which were related to the outcome. Indeed, we observed that an ADC decrease is more evident in animals that would not survive the septic challenge than in surviving animals (Figure 3). This indicates that the induction of cytotoxic edema in the cortical and thalamic areas of the brain is an important component of the pathogenesis of brain dysfunction in sepsis, as shown earlier in the hippocampal region using optical microscopy (Kafa *et al*, 2007). However, we cannot rule out that the cytotoxic edema is present also in other areas of the brain that were not studied in this protocol. Conceivably, the biophysical consequences of this cellular damage alone could be responsible for the decrease in ADC through the nonspecific release of intracellular components in the interstitial milieu. In addition, damaged cells would also be unable to maintain proper regulation of endothelial function. The recent identification of mitochondrial dysfunctions occurring in the septic brain (d'Avila *et al*, 2008), that is, the disruptions in energy metabolism and impaired chemical potential gradients across the mitochondrial membrane, may be mechanistically related to the osmotic imbalance leading to ADC perturbations and thus cytotoxic edema.

Recently it was revealed that little to no changes in ADCs could be detected in early (up to 3.5 h) periods of lipopolysaccharide-induced endotoxemia in rats (Rosengarten *et al*, 2008). This apparent discrepancy could arise from the differences between experimental models (Remick *et al*, 2000). The inflammatory processes mediated by purified lipopolysaccharide cannot *a priori* be expected to match the intensity and diversity of stimuli triggered by polymicrobial sepsis. In addition, the time frames of these studies are dissimilar and no assessments of diffusion coefficients were performed at 6 or 24 h. Incidentally, our findings resemble somewhat the pathogenesis encountered in malaria infections, especially regarding the decreased ADC observed in the cortex (Penet *et al*, 2005). An important point shared between malaria and CLP-induced sepsis is the involvement of inflammatory mediators. Although sepsis and malaria differ substantially in their pathogenesis, both seem to share cerebral edema, but at different intensities, as an important hallmark of these conditions. It is well established that disruptions in the blood–brain barrier integrity are prominent in malaria, where they result in decreased perfusion and edema formation (Lackner *et al*, 2006).

Despite the novelty of our findings, we acknowledge some limitations to our work. Our approach could become more informative if it were merged with hemodynamic observations of brain. One could argue that the observed effects of sepsis in the brain could be secondary to the hemodynamic changes frequently found in sepsis. Despite the fact that we could not monitor blood pressure during the MRI procedure, we think that brain dysfunction has a multifactorial pathophysiology and the precise role of each component, such as, inflammation, apoptosis, hypotension, metabolic alterations, and others is presently uncharacterized. Also, using a pig model of sepsis, Bogdanski *et al* (2000) showed brain perivascular and cytotoxic edema and neuronal death. It is important to notice, however, that hemodynamic and ventilatory parameters were strictly controlled in such a way that oxygen delivery to tissues was not limited (Bogdanski *et al,* 2000). Recently, it was shown that rats subjected to CLP (with a mortality rate of 43%) did not have alterations in mean whole or local brain blood flow and the authors concluded that brain dysfunction is not a consequence of changes of cerebral blood flow during severe sepsis (Hinkelbein *et al*, 2007).

Previous studies by Messaris *et al* (2004) have shown cells with apoptotic morphology in pyramidal cells of the CA1 region of the hippocampus, the cells of the choroid plexus, and the Purkinje cells of the cerebellum by hematoxylin and eosin staining and transmission electron microscopy. These modifications started at 6 h after CLP and increased in the late phases of sepsis. In fact, these authors also showed an increase of bax immunoreactivity in CA1 region of the hippocampus, in choroids plexus, and in Purkinje cells of the cerebellum early at 6 h after CLP and concluded that Bax seems to have an important role in this process, probably by leading cells to death by releasing cytochrome *c* from mitochondria. Similar findings were reported by Papadopoulos *et al* (1999) 8 h after experimental sepsis in pigs. Other studies have also confirmed the presence of apoptosis in the brain after experimental sepsis (Chan *et al*, 2007; Sharshar *et al*, 2004). Although we cannot assure the presence of apoptosis on our experiments, the results of our study indicate that MRI and spectroscopy are suited tools to detect early neuronal injury after sepsis. Obtaining spectra from the base of the brain, particularly single-voxel MRS, is not possible because of the contribution of protons from the surrounding tissue, however chemical shift imaging, in which the spectral information gets spatially encoded, may be a possibility for future studies. Overall, our spectroscopy data corroborate earlier findings, which indicated cell damage accompanied with decreased NAA levels in sepsis (Davies, 2002; Orihuela *et al*, 2006; Papadopoulos *et al*, 1999).

Despite these limitations, the present results highlight the potential that magnetic resonance techniques have in determining the fundamental processes associated with sepsis as well as possibly its response to various therapeutic agents. The development of new magnetic resonance technique of molecularly targeted contrast agents could also be used to monitor the expression of a variety of markers of interest in sepsis pathogenesis. This approach was especially useful in determining the expression profile of the inflammatory mediator, c-Met in the brain of tumor-bearing rats (Towner *et al*, 2008), and could in principle be used in sepsis with only minor modifications. In particular, the acquisition of data regarding oxidative stress markers sensitive to mitochondrial metabolism is currently underway in our group, as the results presented here corroborate earlier findings about sepsis-induced mitochondrial dysregulations (d'Avila *et al*, 2008).

Taken together, these observations indicate that MRI represents a suitable modality to investigate inflammation-mediated complications of the cerebral microvasculature and more generally for the study of brain complications in septic mice. Significant quantitative changes were detected in the metabolic profile, brain basal vasculature integrity, and tissue ADC of septic animals. These previously unreported end points add insight into sepsis pathologic processes, and their quantitative nature may ultimately result in improvements to the accuracy of sepsis diagnostic and severity assessment in patients.

Acknowledgements

FAB, MFO, and HCCFN are research scholars from CNPq.

Conflict of interest

The authors declare no conflict of interest.

References

Anda T, Yamashita H, Khalid H, Tsutsumi K, Fujita H, Tokunaga Y, Shibata S (1997) Effect of tumor necrosis factor-alpha on the permeability of bovine brain microvessel endothelial cell monolayers. *Neurol Res* 19:369–76

Barichello T, Martins MR, Reinke A, Feier G, Ritter C, Quevedo J, Dal-Pizzol F (2005) Long-term cognitive impairment in sepsis survivors. *Crit Care Med* 33:1671

Birken DL, Oldendorf WH (1989) *N*-acetyl-L-aspartic acid: a literature review of a compound prominent in 1H-NMR spectroscopic studies of brain. *Neurosci Biobehav Rev* 13:23–31

Blankenberg FG, Katsikis PD, Storrs RW, Beaulieu C, Spielman D, Chen JY, Naumovski L, Tait JF (1997) Quantitative analysis of apoptotic cell death using proton nuclear magnetic resonance spectroscopy. *Blood* 89:3778–86

Bogdanski R, Blobner M, Becker I, Hanel F, Fink H, Kochs E (2000) Cerebral histopathology following portal venous infusion of bacteria in a chronic porcine model. *Anesthesiology* 93:793–804

Chan JY, Chang AY, Wang LL, Ou CC, Chan SH (2007) Protein kinase C-dependent mitochondrial translocation of proapoptotic protein Bax on activation of inducible nitric-oxide synthase in rostral ventrolateral medulla mediates cardiovascular depression during experimental endotoxemia. *Mol Pharmacol* 71:1129–39

d'Avila JC, Santiago AP, Amancio RT, Galina A, Oliveira MF, Bozza FA (2008) Sepsis induces brain mitochondrial dysfunction. *Crit Care Med* 36:1925–32

Davies DC (2002) Blood–brain barrier breakdown in septic encephalopathy and brain tumours. *J Anat* 200:639–46

Eis M, Els T, Hoehn-Berlage M (1995) High resolution quantitative relaxation and diffusion MRI of three different experimental brain tumors in rat. *Magn Reson Med* 34:835–44

Ely EW, Shintani A, Truman B, Speroff T, Gordon SM, Harrell Jr FE, Inouye SK, Bernard GR, Dittus RS (2004) Delirium as a predictor of mortality in mechanically ventilated patients in the intensive care unit. *JAMA* 291:1753–62

Flierl MA, Stahel PF, Rittirsch D, Huber-Lang M, Niederbichler AD, Hoesel LM, Touban BM, Morgan SJ, Smith WR, Ward PA, Ipaktchi K (2009) Inhibition of complement C5a prevents breakdown of the blood–brain barrier and pituitary dysfunction in experimental sepsis. *Crit Care* 13:R12

Franklin KBJ, Paxinos G (1997) *The Mouse Brain in Stereotaxic Coordinates*. San Diego, CA: Academic Press (Elsevier)

Gomes RN, Bozza FA, Amancio RT, Japiassu AM, Vianna RC, Larangeira AP, Gouvea JM, Bastos MS, Zimmerman GA, Stafforini DM, Prescott SM, Bozza PT, Castro-Faria-Neto HC (2006) Exogenous platelet-activating factor acetylhydrolase reduces mortality in mice with systemic inflammatory response syndrome and sepsis. *Shock* 26:41–9

Gruetter R (1993) Automatic, localized *in vivo* adjustment of all first- and second-order shim coils. *Magn Reson Med* 29:804–11

Hinkelbein J, Schroeck H, Peterka A, Schubert C, Kuschinsky W, Kalenka A (2007) Local cerebral blood flow is preserved in sepsis. *Curr Neurovasc Res* 4:39–47

Huynh HK, Dorovini-Zis K (1993) Effects of interferon-gamma on primary cultures of human brain microvessel endothelial cells. *Am J Pathol* 142:1265–78

Jeppsson B, Freund HR, Gimmon Z, James JH, von Meyenfeldt MF, Fischer JE (1981) Blood–brain barrier derangement in sepsis: cause of septic encephalopathy? *Am J Surg* 141:136–42

Kadoi Y, Goto F (2004) Selective inducible nitric oxide inhibition can restore hemodynamics, but does not improve neurological dysfunction in experimentally-induced septic shock in rats. *Anesth Analg* 99:212–20

Kafa IM, Ari I, Kurt MA (2007) The peri-microvascular edema in hippocampal CA1 area in a rat model of sepsis. *Neuropathology* 27:213–20

Kokubo Y, Matson GB, Derugin N, Hill T, Mancuso A, Chan PH, Weinstein PR (2002) Transgenic mice expressing human copper-zinc superoxide dismutase exhibit attenuated apparent diffusion coefficient reduction during reperfusion following focal cerebral ischemia. *Brain Res* 947:1–8

Lackner P, Beer R, Helbok R, Broessner G, Engelhardt K, Brenneis C, Schmutzhard E, Pfaller K (2006) Scanning electron microscopy of the neuropathology of murine cerebral malaria. *Malar J* 5:116

Lin SM, Huang CD, Liu CY, Lin HC, Wang CH, Huang PY, Fang YF, Shieh MH, Kuo HP (2008) Risk factors for the development of early-onset delirium and the subsequent clinical outcome in mechanically ventilated patients. *J Crit Care* 23:372–9

Messaris E, Memos N, Chatzigianni E, Konstadoulakis MM, Menenakos E, Katsaragakis S, Voumvourakis C, Androulakis G (2004) Time-dependent mitochondrial-mediated programmed neuronal cell death prolongs survival in sepsis. *Crit Care Med* 2004; 32:1764–70

Moffett JR, Ross B, Arun P, Madhavarao CN, Namboodiri AM (2007) *N*-acetylaspartate in the CNS: from neurodiagnostics to neurobiology. *Prog Neurobiol* 81:89–131

Orihuela CJ, Fillon S, Smith-Sielicki SH, El Kasmi KC, Gao G, Soulis K, Patil A, Murray PJ, Tuomanen EI (2006) Cell wall-mediated neuronal damage in early sepsis. *Infect Immun* 74:3783–9

Pancoto JA, Correa PB, Oliveira-Pelegrin GR, Rocha MJ (2008) Autonomic dysfunction in experimental sepsis induced by cecal ligation and puncture. *Auton Neurosci* 138:57–63

Papadopoulos MC, Davies DC, Moss RF, Tighe D, Bennett ED (2000) Pathophysiology of septic encephalopathy: a review. *Crit Care Med* 28:3019–24

Papadopoulos MC, Lamb FJ, Moss RF, Davies DC, Tighe D, Bennett ED (1999) Faecal peritonitis causes oedema and neuronal injury in pig cerebral cortex. *Clin Sci (London)* 96:461–6

Penet MF, Viola A, Confort-Gouny S, Le Fur Y, Duhamel G, Kober F, Ibarrola D, Izquierdo M, Coltel N, Gharib B, Grau GE, Cozzone PJ (2005) Imaging experimental cerebral malaria *in vivo*: significant role of ischemic brain edema. *J Neurosci* 25:7352–8

Pfeuffer J, Tkac I, Provencher SW, Gruetter R (1999) Toward an *in vivo* neurochemical profile: quantification of 18 metabolites in short-echo-time (1)H NMR spectra of the rat brain. *J Magn Reson* 141:104–20

Remick DG, Newcomb DE, Bolgos GL, Call DR (2000) Comparison of the mortality and inflammatory response

of two models of sepsis: lipopolysaccharide vs. cecal ligation and puncture. *Shock* 13:110–6

Rosengarten B, Walberer M, Allendoerfer J, Mueller C, Schwarz N, Bachmann G, Gerriets T (2008) LPS-induced endotoxic shock does not cause early brain edema formation—an MRI study in rats. *Inflamm Res* 57: 479–83

Ross B, Bluml S (2001) Magnetic resonance spectroscopy of the human brain. *Anat Rec* 265:54–84

Server A, Kulle B, Maehlen J, Josefsen R, Schellhorn T, Kumar T, Langberg CW, Nakstad PH (2009) Quantitative apparent diffusion coefficients in the characterization of brain tumors and associated peritumoral edema. *Acta Radiol* 50:682–9

Sharshar T, Annane D, de la Grandmaison GL, Brouland JP, Hopkinson NS, Francoise G (2004) The neuropathology of septic shock. *Brain Pathol* 14:21–33

Sharshar T, Carlier R, Bernard F, Guidoux C, Brouland JP, Nardi O, de la Grandmaison GL, Aboab J, Gray F, Menon D, Annane D (2007) Brain lesions in septic shock: a magnetic resonance imaging study. *Intensive Care Med* 33:798–806

Sharshar T, Gray F, Lorin de la Grandmaison G, Hopkinson NS, Ross E, Dorandeu A, Orlikowski D, Raphael JC, Gajdos P, Annane D (2003) Apoptosis of neurons in cardiovascular autonomic centres triggered by inducible nitric oxide synthase after death from septic shock. *Lancet* 362:1799–805

Siami S, Annane D, Sharshar T (2008) The encephalopathy in sepsis. *Crit Care Clin* 24:67–82, viii

Sibtain NA, Howe FA, Saunders DE (2007) The clinical value of proton magnetic resonance spectroscopy in adult brain tumours. *Clin Radiol* 62:109–19

Sprung CL, Peduzzi PN, Shatney CH, Schein RM, Wilson MF, Sheagren JN, Hinshaw LB (1990) Impact of encephalopathy on mortality in the sepsis syndrome. The Veterans Administration Systemic Sepsis Cooperative Study Group. *Crit Care Med* 18:801–6

Stejskal EO, Tanner JE (1965) Spin diffusion measurements—spin echoes in presence of a time-dependent field gradient. *J Chem Phys* 42:288–92

Testylier G, Lahrech H, Montigon O, Foquin A, Delacour C, Bernabe D, Segebarth C, Dorandeu F, Carpentier P (2007) Cerebral edema induced in mice by a convulsive dose of soman. Evaluation through diffusion-weighted magnetic resonance imaging and histology. *Toxicol Appl Pharmacol* 220:125–37

Towner RA, Smith N, Doblas S, Tesiram Y, Garteiser P, Saunders D, Cranford R, Silasi-Mansat R, Herlea O, Ivanciu L, Wu D, Lupu F (2008) *In vivo* detection of c-Met expression in a rat C6 glioma model. *J Cell Mol Med* 12:174–86

Vuori K, Kankaanranta L, Hakkinen AM, Gaily E, Valanne L, Granstrom ML, Joensuu H, Blomstedt G, Paetau A, Lundbom N (2004) Low-grade gliomas and focal cortical developmental malformations: differentiation with proton MR spectroscopy. *Radiology* 230:703–8

Walker PM, Ben Salem D, Lalande A, Giroud M, Brunotte F (2004) Time course of NAA T2 and ADC(w) in ischaemic stroke patients: 1H MRS imaging and diffusion-weighted MRI. *J Neurol Sci* 220:23–8